Supplementary information

Clément Pellet-Mary, 1,* Debarghya Dutta, 1,† Märta A. Tschudin, 1,† Patrick Siegwolf, 1
Boris Gross, 1,2 David A. Broadway, 3 Jordan Cox, 4 Carolin Schrader, 1,5 Jodok
Happacher, 1 Daniel G. Chica, 4 Cory R. Dean, 6 Xavier Roy, 4 and Patrick Maletinsky 1,‡

1 Department of Physics, University of Basel, Basel, Switzerland
2 Swiss Nanoscience Institute, University of Basel, 4056 Basel, Switzerland
3 School of Science, RMIT University, Melbourne, VIC 3001, Australia
4 Department of Chemistry, Columbia University, New York, NY, USA
5 Laboratoire Charles Coulomb, Université de Montpellier and CNRS, 34095 Montpellier, France
6 Department of Physics, Columbia University, New York, NY, USA
(Dated: September 22, 2025)

CONTENTS

I.	Sample AFM data	2
II.	Magnetic imaging	3
III.	Large scale imaging	4
IV.	Micromagnetic simulations field evolution	5
V.	Spin-flip transitions in few-layers CrSBr	6
VI.	Field history	7
VII.	Contact angle and wetting analogy	8
VIII.	Additional contact angles and domain wall examples	9
IX.	Second sample	10
	References	11

^{*} clement.pellet-mary@unibas.ch; These authors contributed equally

[†] These authors contributed equally

[‡] patrick.maletinksy@unibas.ch

I. SAMPLE AFM DATA

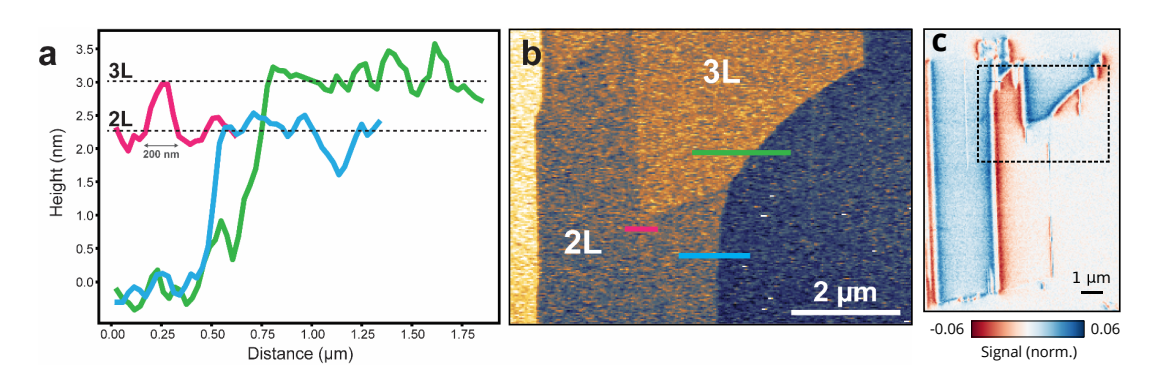


FIG. S1. **a** Atomic force microscopy (AFM) height profiles across 2L (blue), 3L (green) step edges, and small 3L area of interest (red). **b** AFM image with location of height profiles marked in corresponding colors. **c** Dual-Iso-B magnetic imaging of the flake showing the region probed by AFM

II. MAGNETIC IMAGING

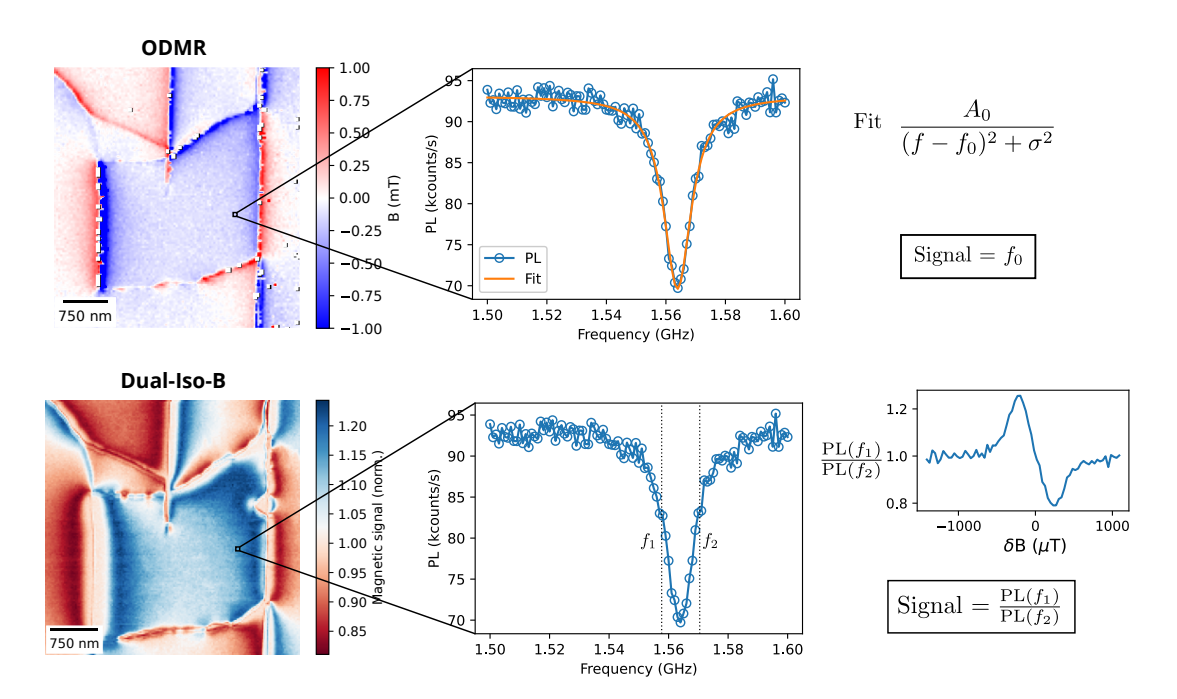


FIG. S2. Example of Dual-Iso-B and ODMR magnetic imaging for similar experimental conditions.

Magnetic imaging of our sample is performed using two sensing schemes - Optically Detected Magnetic resonance (ODMR) and Dual Iso-Magnetic field measurement.

In an ODMR measurement, we continuously excite our NV with a green laser (532nm) and record the photoluminescence (PL) response while driving the spin transition (typically the $m_s = 0$ to $m_s = -1$ transition) using our microwave (MW) source. On resonance, there is a dip in the PL as the NV population is transferred to the darker spin state. The position of this dip is proportional to the magnetic field along the NV-axis. In the vicinity of our sample, the position of this dip changes since the net effective magnetic field is modified, enabling us to extract quantitatively the magnetic contribution from the sample. As we scan over the sample, we measure the ODMR at every point, perform a Lorentzian fit to the spectrum and obtain the additional shift due to the sample. Consequently, we obtain a quantitative measurement of the magnetic stray field from the sample as shown in fig. S2 a.

Measuring the ODMR spectrum at all points during a scan is time intensive and inefficient as most of the measured points have a weak sensitivity to a change in magnetic field. Dual-Iso-B imaging provides a faster(and therefore more sensitive) measurement scheme. In this technique, an IQ mixer is used to modulate the MW source and generate a lower frequency (f1) and higher frequency (f2) drives, usually with f2-f1 as the width of the ODMR. Independent readout of the two PL values at f1 and f2 and normalizing leads to a single spectrum. Away from the sample, we set the applied frequency such that the measured signal S = PL(1)/PL(2) = 1. In the vicinity of the sample, we observe a shift in S, which can be directly translated to the additional magnetic field from the sample. However, if the stray field from the sample is large, the signal S can be beyond the linear regime of the spectrum. In such a case, this method is no longer quantitative but only provides a qualitative picture based on the direction of the shift of the signal S (Fig. S2 b).

In our experiments, we combine both the quantitative full-ODMR imaging and the qualitative Dual-Iso-B imaging to study the magnetic behavior of CrSBr in different scenarios. In this manuscript, ODMR maps and Dual-IsoB maps are color-coded in the same fashion as shown in Fig.S2.

To determine the magnetization state from the stray field imaging (either Dual-Iso-B or ODMR), we analyze the stray field sign and magnitude at the edges of the flake and domain walls as explained in previous works. ^{1,2} Specifically, the stray field profile from the left edge of the bilayer to the substrate yields a magnetisation of zero in the AF region and a magnetisation corresponding to two monolayer magnetisations pointing in the direction of the magnetic field. Conversely, considering the step between the substrate and the bilayer and the bilayer to the pinning layer, yields the magnetisation strengths and directions of these two layers, respectively.

III. LARGE SCALE IMAGING

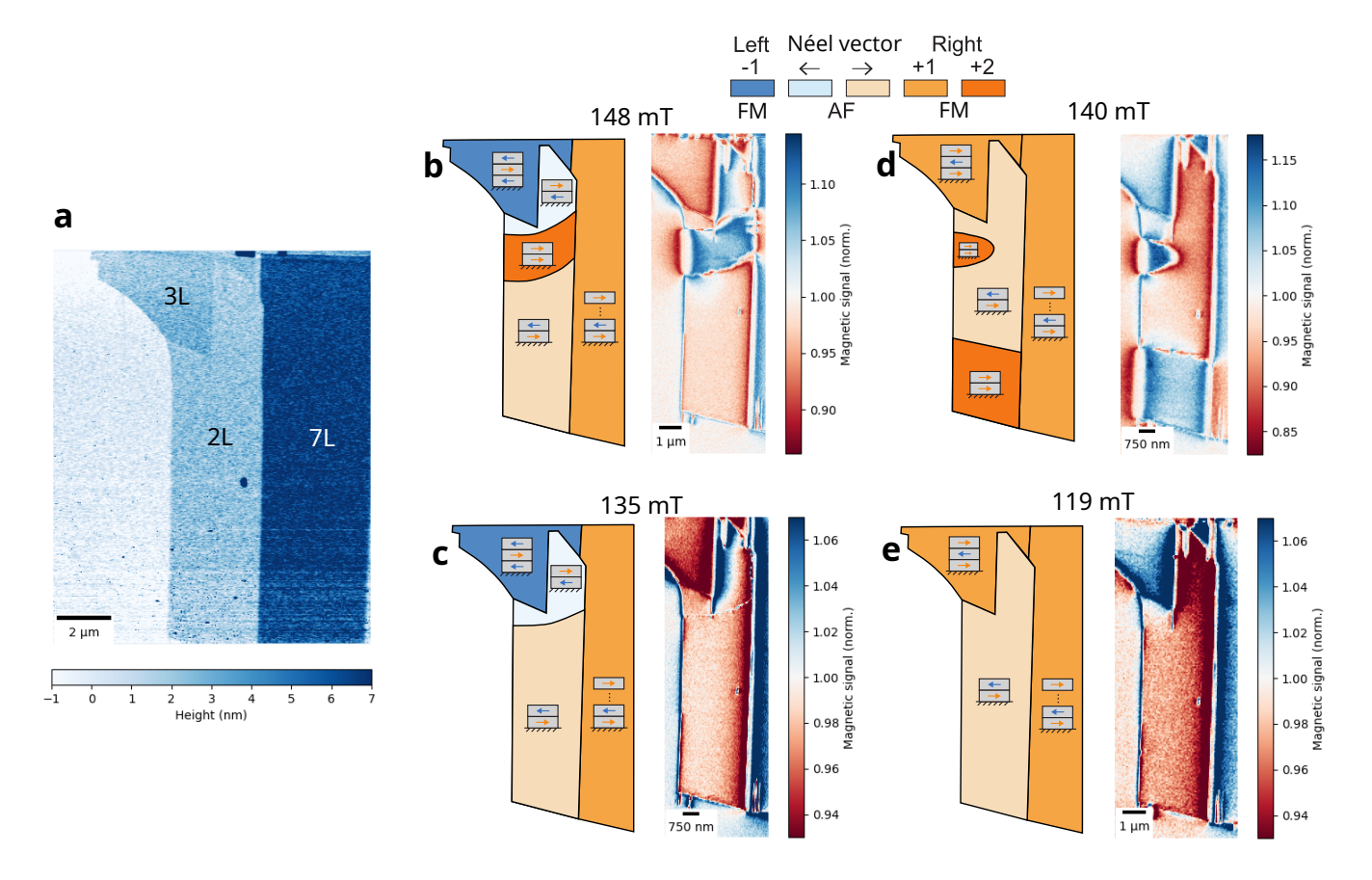


FIG. S3. Large scale images of the bilayer and the adjacent control and pinning layers. **a** AFM height profile of the flake. **b-e** Dual-Iso-B magnetic images of the bilayer, and schematics of the underlying magnetization, for a configuration with an inverted control layer (**b,c**) or a parallel control layer (**d,e**) and different values of the external field.

Most of the magnetic images in this manuscript focus on specific regions of interest. We show here magnetic imaging of the entirety of the bilayer in different cases.

Fig.S3 a presents an AFM height profile of the three relevant stacks to this study (bilayer, trilayer and 7-layer), showing no visible structural defects and clean boundaries between the stacks.

Fig.S3 \mathbf{b} and \mathbf{c} show magnetic imaging of the flake for an inverted control layer (in a similar configuration to Fig.3 \mathbf{b} of the main text), for external field values of 148 mT, where part of the bilayer has flipped into a FM stacking configuration, and 135 mT where the bilayer is split into two AF domains. These images show in particular that no magnetic textures form in the bottom part of the bilayer, as is expected by the fact that this bottom part only shares a boundary with the 7-layer.

Fig.S3 b and c show magnetic imaging of the flake for a control layer aligned with the pinning layer (in a similar configuration to Fig.3 d of the main text). For an external field value of 140 mT, two regions of the bilayer show FM stacking configuration. Both of these domains collapse as the field is lowered to 119 mT, leaving the flake as a uniform, single AF domain.

IV. MICROMAGNETIC SIMULATIONS FIELD EVOLUTION

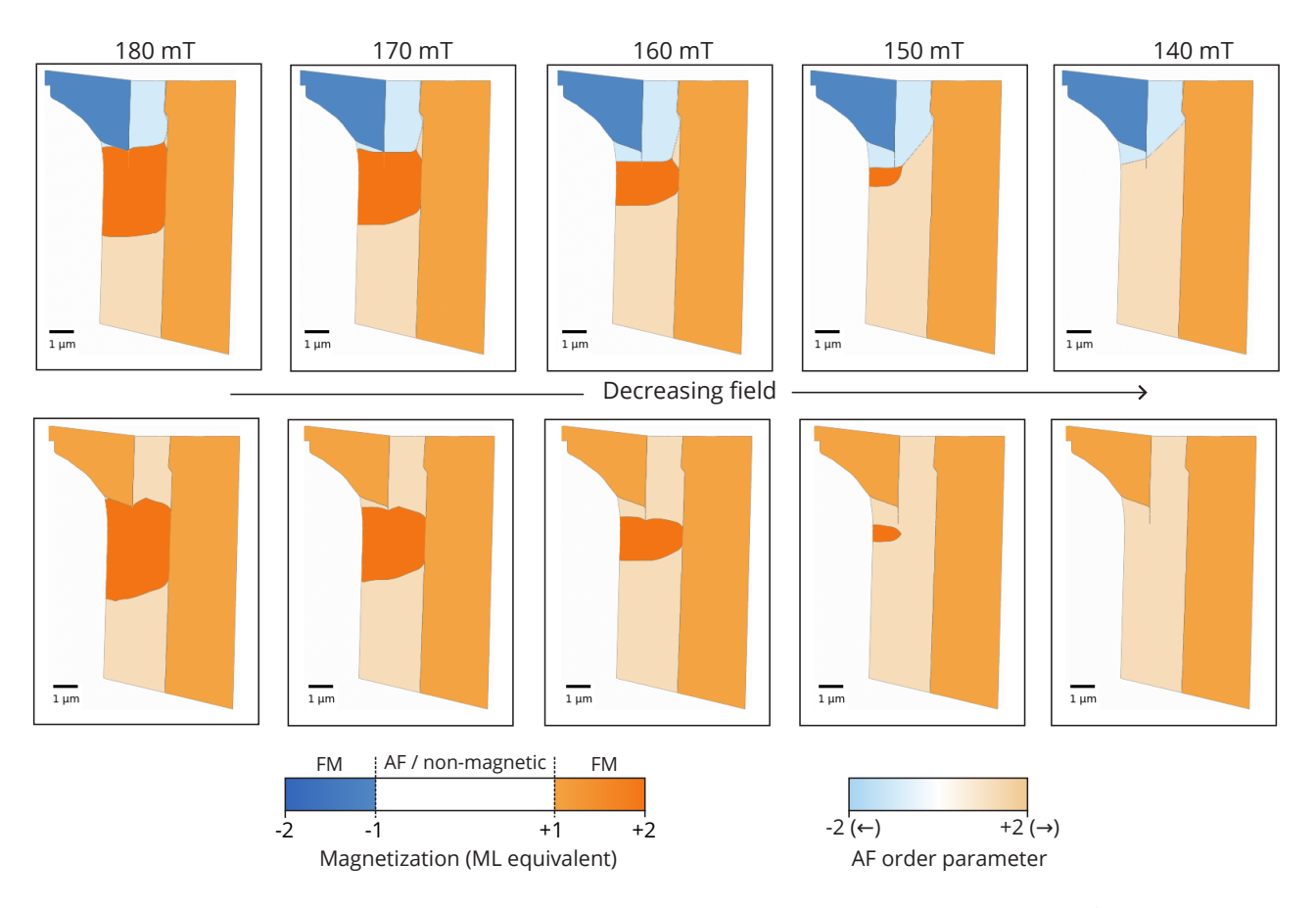


FIG. S4. Micromagnetics simulations for decreasing external field. In order to represent both the FM and AF order, a threshold is applied and two distinct color scales are used. The total magnetization $(M_{1L} + M_{2L} + M_{3L})$ is plotted when its absolute value is superior to 0.9, otherwise, the AF order parameter $(M_{1L} - M_{2L} + M_{3L})$ is plotted, where M_{nL} refers to the relative magnetization along the x-axis of the n-th layer.

V. SPIN-FLIP TRANSITIONS IN FEW-LAYERS CRSBR

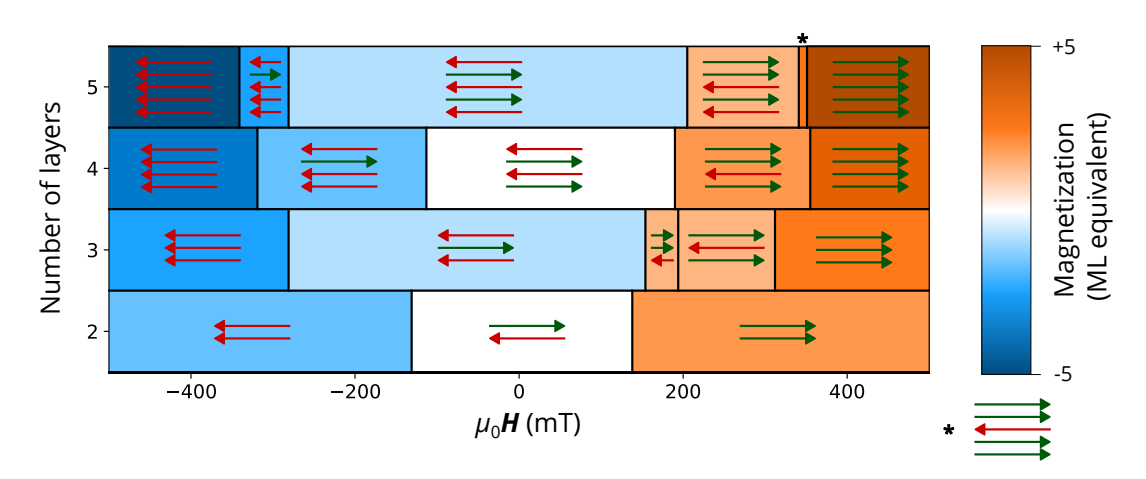


FIG. S5. Spin-flip transition in few layers CrSBr. Arrows represent the magnetization of each layer while background color represent the total magnetization of the flake.

Fig.S5 represents the values of spin-flip transition reported in the literature. Bilayer spin-flip values where found in Wilson et al., trilayer in Tabataba-Vakili et al. and 4 and 5-layer in Liu et al.

Exact values for the spin flip of a given stack differ from study to study. For instance, Wilson et al. reports flipping value between 130 and 140 mT for a bilayer, while Tabataba-Vakili et al. reports values up to ~ 160 mT. These discrepancies could be explain by many factors, such as strain, lack of nucleation sites, or lateral exchange bias.

Particularly relevant for this work or the two arrangements of the trilayer $(\leftarrow/\to/\to)$ and $(\to/\leftarrow/\to)$ that were reported in.⁴ These two stacking orders have the same total magnetization of $-1~M_{ML}$ and are therefore indistinguishable by a magnetometry measurement. In our experiments however, both the contact angles and the presence or absence of an AF domain wall seemed to indicate that trilayer was systematically in the $(\to/\leftarrow/\to)$ or $(\leftarrow/\to/\leftarrow)$ state.

VI. FIELD HISTORY

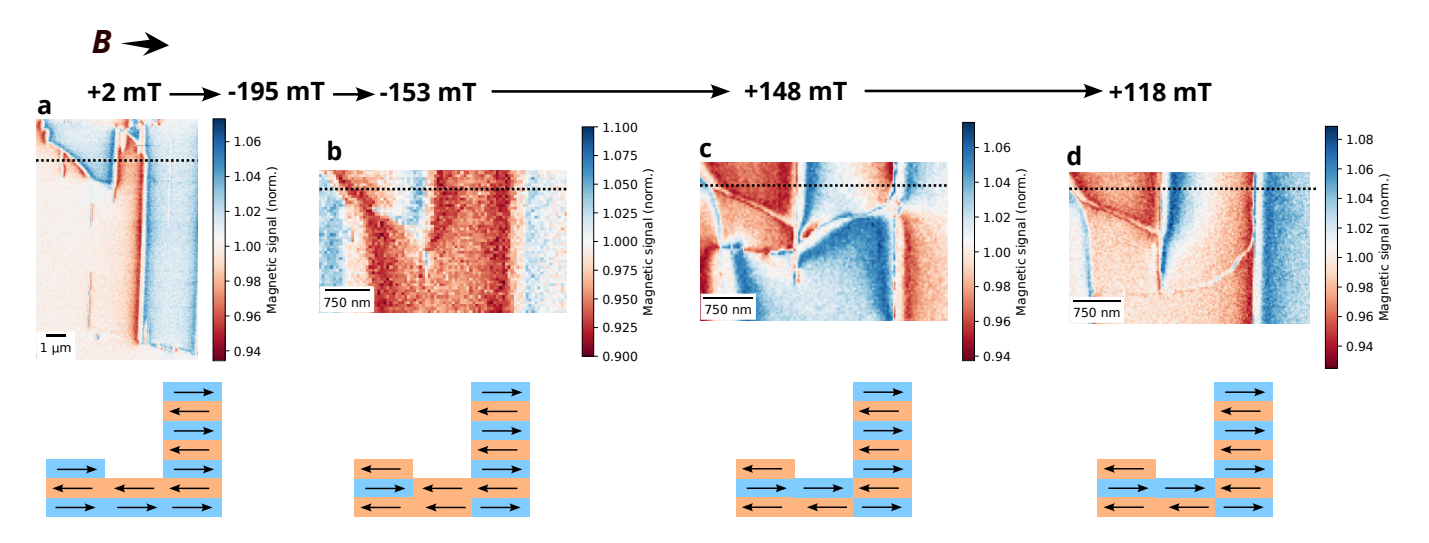


FIG. S6. Initialization sequence of external magnetic fields for the creation of the domain wall. Dual-Iso-B magnetic imaging and schematics of the magnetization for a cross-section (dashed line) are provided for the in-plane field values +2 mT (a), -153 mT (b), +148 mT (c) and +118 mT (d)

Fig.S6 details one of the field cycle used to create an AF domain wall in the bilayer. The flake is first initialized so that each layer is uniformly magnetized. This is achieved either by field cooling or by applying a strong ($\sim 400 \text{ mT}$) in plane positive field. Then a negative field of -195 mT is applied in order to flip the trilayer without flipping the 7-layer. Following this, we apply a positive field of +148 mT, near the bilayer spin-flip transition in order to assess the AF order by using the contact angle (see bellow) formed by the phase wall. If two different AF orders are observed, the field is then reduced to +118 mT in order to observe a domain wall.

In this scheme, it is not strictly necessary to switch from negative to positive field between step **b** and **c**, the domain wall should be present as soon as the bilayer is flipped back to AF order (≈ -140 mT). However for consistency, we always measure the domain wall with positive fields. Similarly, step **c** is technically facultative as the domain wall could be observed directly. However, since the stray field from the AF domain wall is much weaker than that of the AF/FM phase wall, it is easier to look for the deformations of the phase wall in order to assess whether or not a domain wall will be produced.

VII. CONTACT ANGLE AND WETTING ANALOGY

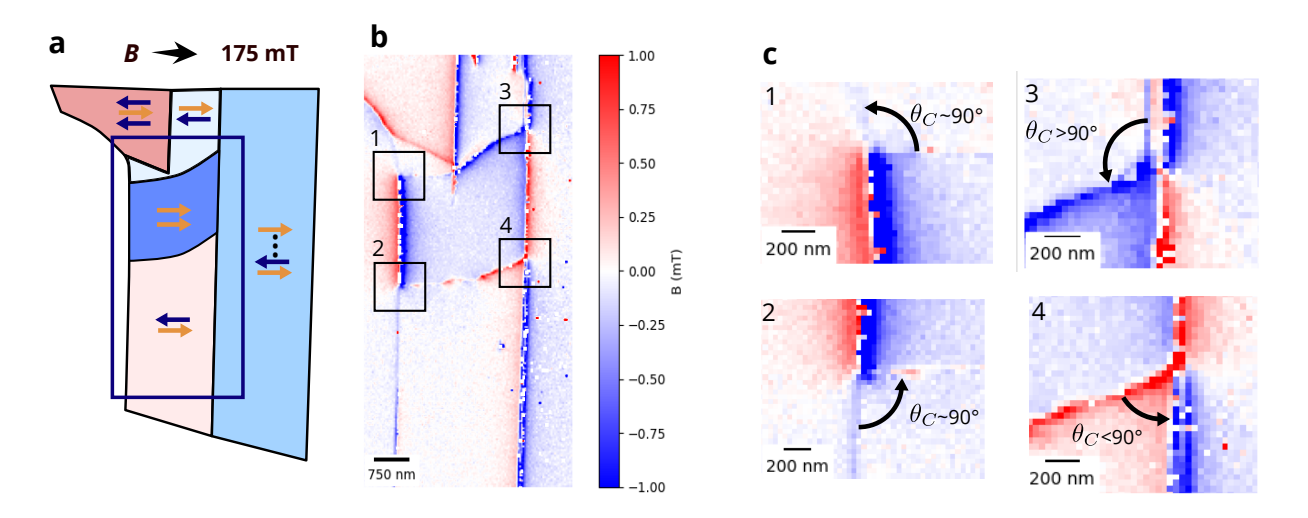


FIG. S7. Contact angles at the bilayer—pinning layer interface. a Schematics of the flake's magnetization. b ODMR magnetic imaging of the flake. c ODMR magnetic zoom in on the four corners of the FM region.

The distortions of the phase walls described in Fig. 2 of the main text can be seen as a form of "contact angle" in an analogy with the phenomenon of wetting in hydrostatics. Indeed, we can assign a surface energy cost at each of the 3 interfaces (AF bilayer–pinning layer, FM bilayer–pinning layer and AF bilayer–FM bilayer), similarly to how wetting is defined by the surface energy between the liquid phase, the gas phase and the substrate.

It should be noted that the analogy between our observations and wetting is not perfect. For one, dipolar field (which is a long range interaction) plays a significant role in the shape of the domains, whereas surface tension is only defined by local interactions. Secondly, the volume of each phase (AF and FM) is not preserved in our experiments, unlike incompressible liquids.

Fig. S7 shows ODMR maps of the sample in the state described in Fig. 2 a-d of the main text, with a focus on the four corners of the FM phase. For the two left-most corners (1 and 2), a contact angle of $\sim 90^{\circ}$ can be observed. This configuration is expected in the absence of LEB as it minimizes both exchange energy ⁷ and dipolar energy (since the phase wall runs parallel to the magnetization of the FM phase).

The two right-most corners however show clearly $\theta_C \neq 90^\circ$, as observed by the strong stray field on the phase wall. These two angles, and their opposite deviation from $\theta_C = 90^\circ$, have been explained in the main text as a consequence of the Néel order in each AF regions and the LEB exerted by the pinning layer. Following with the wetting analogy, we can define angle 3 ($\theta_C > 90^\circ$) as "hydrophobic" because of the high surface energy between the AF phase and the pinning layer, and reversely angle 4 ($\theta_C < 90^\circ$) as "hydrophilic".

VIII. ADDITIONAL CONTACT ANGLES AND DOMAIN WALL EXAMPLES

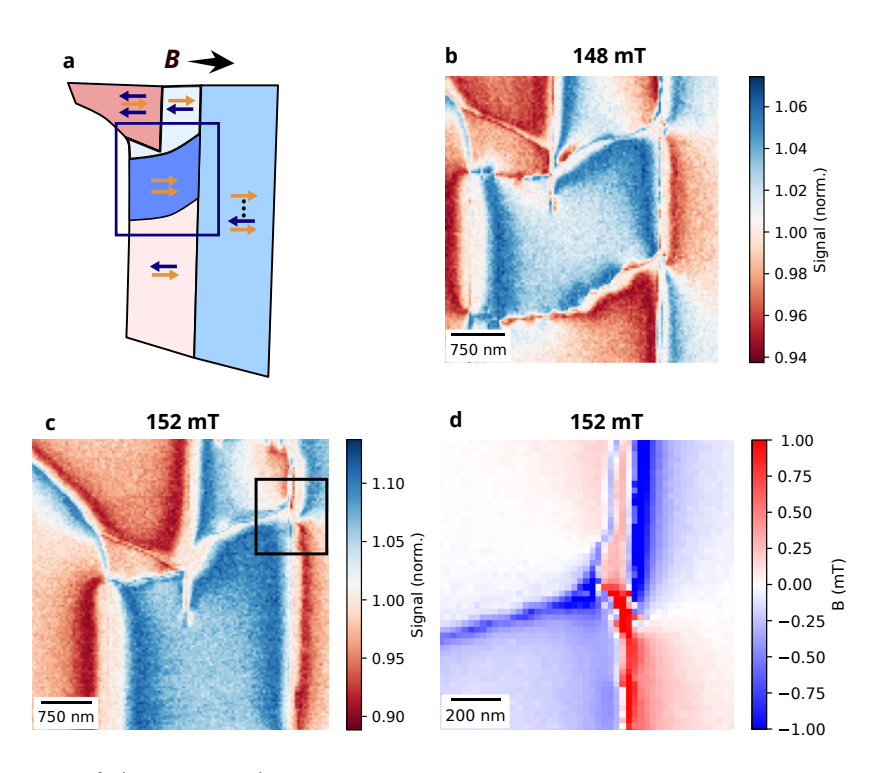


FIG. S8. Example of $\theta_C > 90^{\circ}$ (hydrophobic) contact angles. **a** Schematics of flake magnetization. **b** Dual-Iso-B magnetic imaging for an external in plane field of 148 mT. **c** Dual-Iso-B magnetic imaging for an in plane field of 152 mT after a different magnetic cycle. **d** ODMR magnetic imaging zoom-in from **c**.

This section covers more examples of contact angles and AF domain walls.

Fig. S8 b and c show magnetic images of the flake in the same condition as Fig.2,b of the main text after two distinct LEB cycles. In both cases, we can observe a $\theta_C > 90^{\circ}$ (hydrophobic) angle between the top AF domain, the FM region and the pinning layer.

Fig. S8 d reveals a more complex internal structure to the hydrophobic contact angle. Similarly to the micromagnetics simulations (see section IV), we can observe that a small AF domain of Néel vector \rightarrow (aligned with the pinning layer) forms along the edge of the pinning layer. We can observe the AF domain wall propagating vertically along the 7-layer edge in both Fig. S8 c and d. As a result, there is a small internal hydrophilic contact angle inside the "macroscopic" hydrophobic wetting angle. The same behavior can be seen in Fig.3 b of the main text.

Fig.S9 b and d show more examples of $\theta_C < 90^\circ$ (hydrophilic) contact angles. For these two series, an in-plane field of ~ 300 mT was first applied to create a homogeneous magnetization in all the layers. As a result, the two contact angles visible in Fig.S9 b and the 3 visible in Fig.S9 d are all hydrophilic. Unlike the hydrophobic case, the zoomed-in scans c and e do not reveal any internal structure for these hydrophilic angles.

Finally, Fig.S10 shows the AF domain wall obtained after 4 different iterations of the LEB protocol. The position of the domain wall is shifted from one iteration to the other, but the overall shape is consistent. In particular, we can observe an angle minimizing the surface between the pinning layer and the AF2 domain (top). We can also see a vertical domain wall propagating along the bilayer/7-layer edge, similar to what we described in Fig.S8.

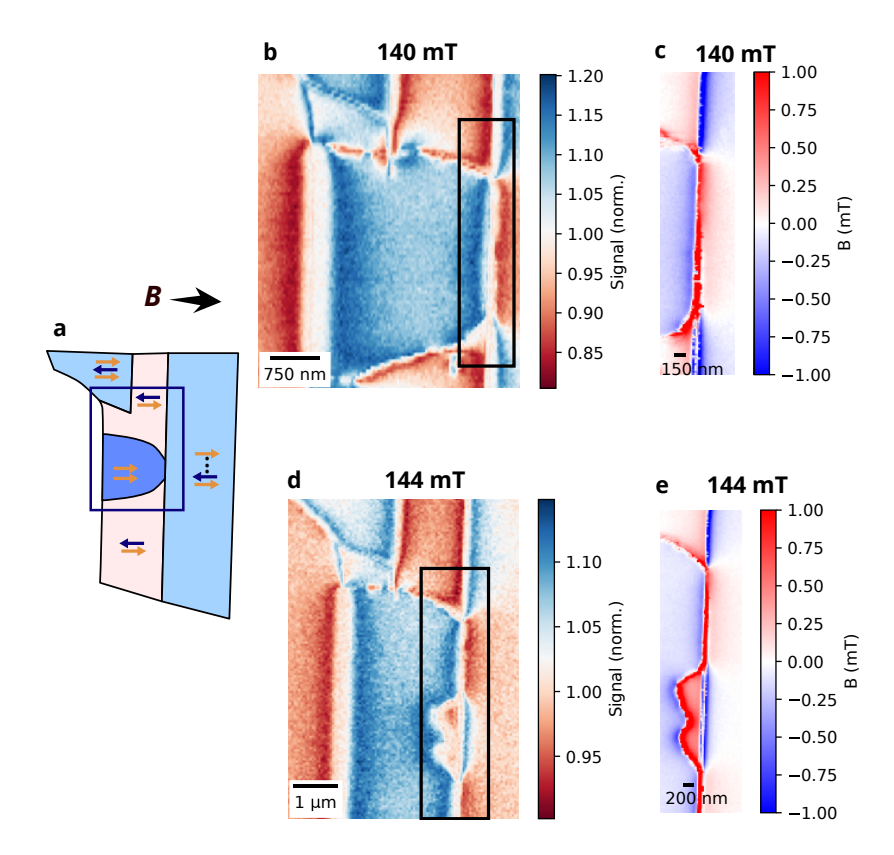


FIG. S9. Example of $\theta_C < 90^{\circ}$ (hydrophilic) contact angles on sample S_1 . a Schematics of flake magnetization. **b(d)** Dual-Iso-B magnetic images for an external in-plane field of 140(144) mT after two different magnetic cycles. **c(e)** ODMR magnetic image zoom-in from **b(d)**.

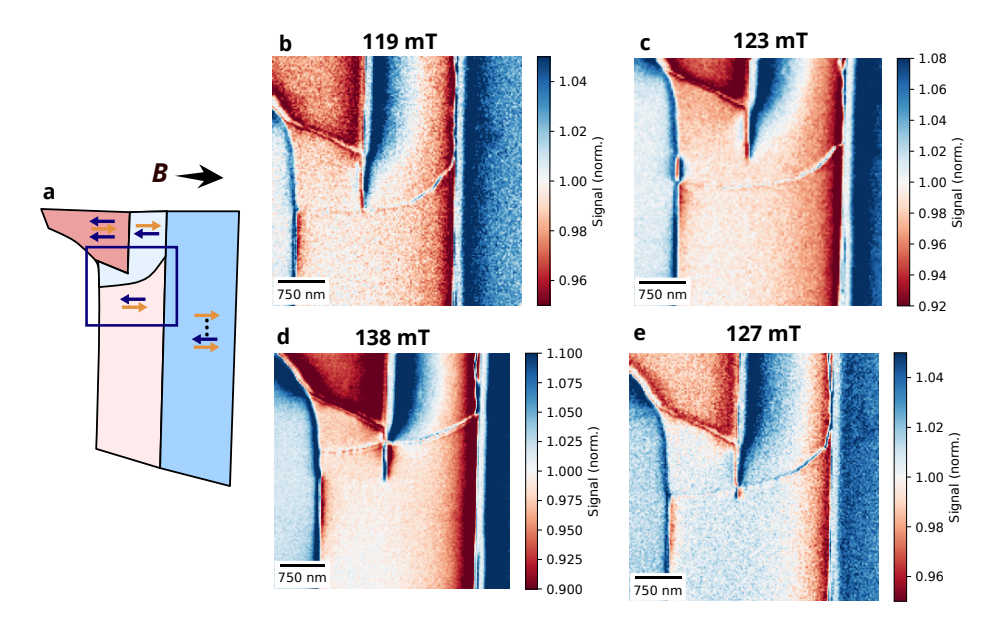


FIG. S10. Example of domain walls on sample S_1 . **a** Schematics of the flake and layer stacking order. **b,c,d,e** Dual-Iso-B images for 4 different LEB cycles. **d** corresponds to Fig. 4 **a** from main text.

IX. SECOND SAMPLE

The LEB protocol described in main text was applied to a second sample that we name S_2 . An optical image of this sample is shown in Fig. S11 a. The relevant stacks for this study are the bottom trilayer and the bilayer directly

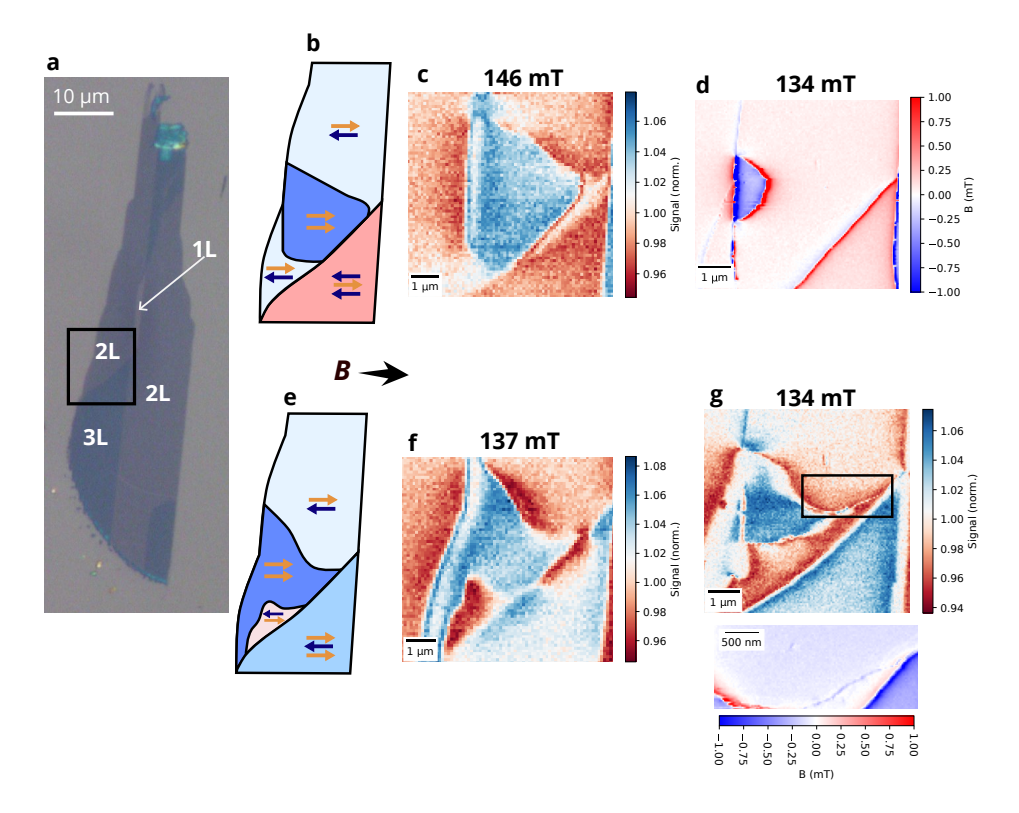


FIG. S11. Lateral exchange bias on sample S_2 . a Optical image of the flake with stacks of 1, 2 and 3 layers being labeled. b Schematics of the layers stacking order for the left bi- and trilayer (trilayer in the AF $M_S = -1$ ML state.) c Dual-Iso-B magnetic imaging (scanning window as a black rectangle in a) of the flake for an external in plane field of 146 mT and the trilayer in the AF $M_S = -1$ ML state. d ODMR magnetic imaging of the flake for an external in plane field of 134 mT and the trilayer in the AF $M_S = -1$ ML state. e Same as b with the trilayer in the AF $M_S = +1$ ML state. f Dual-Iso-B magnetic image of the flake for an external in plane field of 137 mT and the trilayer in the AF $M_S = +1$ ML state. g (top) Dual-Iso-B magnetic imaging of the flake for an external in plane field of 134 mT and the trilayer in the AF $M_S = +1$ ML state. (bottom) ODMR magnetic image of the window shown on the the top image

on top. Similarly to the flake presented in main text, when applying an external field close to the bilayer spin-flip transition, the bilayer is split into a central FM region and a top and a bottom AF regions.

Fig. S11 b,c and d represent the case where the trilayer is in its $M_S = -1$ ML AF state. Both contact angles visible in Fig. S11 c are $< 90^{\circ}$, meaning that both top and bottom regions have a Néel vector \rightarrow . This is confirmed in Fig. S11 d by reducing the external field and observing that no domain wall appears.

On the other hand, Fig. S11 **e**,**f** and **g** represent the case where the trilayer is in its $M_S = +1$ ML AF state (flipped by applying a +180 mT in plane field). There, the contact angle formed by the bottom AF region is $< 90^{\circ}$, but the one formed by the top one is $> 90^{\circ}$. The top region therefore has a Néel vector \leftarrow , and the bottom region \rightarrow . This is again confirmed in Fig. S11 **g** by reducing the field and observing the appearance of a domain wall between the two AF domains.

In both cases, the bottom AF region seems to nucleate from the trilayer boundary, which explains why it changed its order parameter when the trilayer was flipped. The top domain AF however nucleates outside of the scanning window. We expect that it nucleates from some of the thicker flakes visible on the top of the optical image, as applying fields up to 300 mT was not enough to switch its AF order.

^[1] Thiel, L. et al. Probing magnetism in 2d materials at the nanoscale with single-spin microscopy. Science 364, 973 (2019).

^[2] Tschudin, M. A. et al. Imaging nanomagnetism and magnetic phase transitions in atomically thin CrSBr. Nat. Commun. 15, 1–10 (2024).

^[3] Wilson, N. P. et al. Interlayer electronic coupling on demand in a 2D magnetic semiconductor. Nat. Mater. 20, 1657–1662 (2021).

^[4] Tabataba-Vakili, F. et al. Doping-control of excitons and magnetism in few-layer CrSBr. Nat. Commun. 15, 1–9 (2024).

- $[5] \ \text{Liu, Z. } \textit{et al.} \ \text{Probing spin textures in atomically thin CrSBr through tunneling magnetoresistance.} \ \textit{arXiv} \ (2024). \ 2407.13230.$
- [6] Cenker, J. et al. Reversible strain-induced magnetic phase transition in a van der Waals magnet. Nat. Nanotechnol. 17, 256–261 (2022).
- [7] Hubert, A. & Schäfer, R. Magnetic domains: the analysis of magnetic microstructures (Springer Science & Business Media, 2008).